Elevated Amygdala Perfusion Mediates Developmental Sex Differences in Trait Anxiety

Supplemental Information

Supplementary Methods 2
Clinical Assessment 2
STAI Factor Analyses 2
Image Data Acquisition 3
Image Processing 4
Cerebral Blood Flow Quantification 5
Group-level Analyses 6
Analyses of Interactions With Age and Puberty 7
Mediation Analysis 7
Sensitivity Analyses 8
Connectivity Analyses 8
Table S1. Sample size for each pubertal stage. 11
Table S2. Factor loadings on the state summary factor of the State-Trait Anxiety Inventory 12
Table S3. Factor loadings on the trait summary factor of the State-Trait Anxiety Inventory 13
Table S4. Regions where trait anxiety was associated with increased perfusion using a more liberal cluster threshold. 14
Table S5. Voxelwise analyses with state and trait anxiety modeled separately. 15
Table S6. Sensitivity analyses with race, maternal level of education, and no psychiatric psychotropic medications 16
Table S7. Regions where raw scores on trait anxiety were associated with increased perfusion. 17
Table S8. Differences in CBF between categorical screening groups and typically developing youth within the left amygdala cluster. 18
Figure S1. State and trait anxiety by screening diagnostic category. 19
Figure S2. Lower perfusion associated with head motion. 20
Supplementary References 21

SUPPLEMENTARY METHODS

Clinical Assessment

As described in detail elsewhere (1-4), assessment of lifetime psychopathology was conducted using a structured screening interview (GOASSESS) based on a modified version of the Kiddie-Schedule for Affective Disorders and Schizophrenia (5). Screening categories were determined using the Diagnostic and Statistical Manual of Mental Disorders, 4th edition, Text Revision criteria (6). Demographic data by screening category are summarized in **Table 1**. The median interval between clinical assessment and neuroimaging was 2 months. Pubertal status was evaluated using an abbreviated version of a computerized, privately administered self-report measure of pubertal traits (7). As for prior work in this dataset (8), puberty was coded as a categorical variable with three classes: early pubertal (Tanner stages 1-3), mid-pubertal (Tanner stage 4), and post-pubertal (Tanner stage 5). For the number of individuals in each pubertal group, see supplementary **Table S1**.

STAI Factor Analyses

The clinical assessment screened for current and lifetime symptoms on a categorical basis. However, the timing of the clinical assessment using GOASSESS did not coincide with the time of imaging. In order to dimensionally evaluate both the overall propensity for anxiety and mood symptoms as well as their presence at the time of imaging, participants additionally completed the STAI immediately prior to their scan. Notably, previous factor analyses of STAI data have demonstrated the presence of a response bias to reverse coded items that varies across individuals and is not related to symptoms (9,10). Factor analyses were conducted separately for the state and trait anxiety items in order to reduce response bias to reverse coded items. To

remove the influence of such effects, we conducted two separate factor analyses of the items in the state and trait scales (see **Table S2** and **S3** for the factor loadings). Following initial exploratory factor analyses, which demonstrated the presence of correlated traits in each scale, confirmatory bifactor analyses (11,12) using a mean- and variance-adjusted weighted least squares estimator in MPlus (13) were used to allow each item to load onto a summary factor (representing trait or state anxiety) as well factors related to response bias (1,14). As anticipated by prior work (9), this approach yielded a summary factor for trait anxiety and a summary factor for state anxiety as well as two specific factors related to response bias, which were not considered further. Due in part to the removal of non-specific response bias effects, trait and state summary scores were less related than raw state and trait total scores (r^2 = .24 versus r^2 = .33). For regions where raw scores on trait anxiety (not factor analyzed to remove response bias) were associated with increased perfusion, see **Table S7**.

Image Data Acquisition

A magnetization-prepared rapid acquisition gradient echo T1-weighted image (TR 1810 ms; TE 3.51 ms; TI 1100 ms; FOV 180 × 240 mm; matrix 192 × 256; 160 slices; slice thickness/gap 1/0 mm; flip angle 9°; GRAPPA 2; effective voxel resolution 0.9 × 0.9 × 1 mm; total acquisition time 3:28 min) was acquired for spatial normalization to standard atlas space. A B0 field map using a double-echo gradient recall echo sequence (TR 1000 ms; TE1 2.69 ms; TE2 5.27 ms; 44 slices; slice thickness/gap 4/0 mm; flip angle 60°; FOV 240 mm; effective voxel resolution 3.8 × 3.8 × 4 mm; total acquisition time 1:04 min) was used for distortion correction procedures. Brain perfusion was imaged using a custom written pseudo-continuous arterial spin labeling (pCASL) sequence (15). The sequence used a single-shot spin-echo EPI readout with the following

parameters: TR 4 s, TE 15 ms, flip angle 90/180°, FOV 220 × 220 mm, matrix 96 × 96 × 20, slice thickness/gap 5/1 mm, effective voxel resolution 2.3 × 2.3 × 6 mm, label duration 1,500 ms, post-label delay 1,200 ms, GRAPPA 2, 80 volumes (40 label, 40 control). Total acquisition time was 5 minutes, 32 seconds. To avoid slice ordering confounds, slice acquisition involved an ascending, non-interleaved order. Slices were acquired in a compressed scheme rather than distributing the slice acquisitions evenly throughout the TR period so that all slices have a similar post-label delay. All scans were obtained in on the same scanner, using the same sequences, and the same head coil, without any major hardware upgrades over the course of the study.

Image Processing

Data was processed with FSL (16) using standard procedures including skull removal with BET (17), slice time correction, motion-correction with MCFLIRT (18), spatial smoothing (6 mm FWHM), mean-based intensity normalization, coregistration to the T1 image using boundary-based registration (19), distortion correction using FUGUE, and normalization to the Montreal Neurologic Institute 152 1 mm template using the top-performing diffeomorphic SyN registration of ANTs (20,21). Due to a frequency-dependent lipid artifact in the present spin-echo pCASL data, as in all prior work using PNC ASL data, the last four image pairs of the series were discarded. Images were down-sampled to 2-mm resolution prior to group-level analysis. Transformations were concatenated and only one interpolation was performed.

In-scanner head motion was evaluated using the re-alignment parameters estimated with FSL's MCFLIRT routine (16). A motion transformation matrix is derived for each time point and six motion parameters (three translations and three rotations) are used to describe each

transform. From this six parameter timeseries, a single vector is created representing the root mean squared volume-to-volume displacement of all brain voxels (18). This motion timeseries can then be used to measure the RMS displacement relative to a single reference volume (absolute displacement) or relative to the preceding volume (relative displacement). Consistent with our previous work (22,23), we used the relative RMS displacement as a measure of motion for both the ASL and the resting-state fMRI scans (see below). The motion timeseries was concisely summarized by computing the mean relative displacement, which is the mean value of the relative displacement vector. Of note, we found that head motion was correlated with age (r = -.15, p < .001) and with CBF in the left amygdala (r = -.14, p < .001), left insula (r = -.03, p = .02), right insula (r = -.04, p = .005), but not the fusiform (r = .01, p = .49). Notably, motion during the ASL scan was ***not*** correlated with trait anxiety (r = -.01, p = .86).

Cerebral Blood Flow Quantification

ASL uses electromagnetically labeled water in arterial blood as an endogenous tracer for quantifying CBF (24,25). Prior research has demonstrated that CBF itself is tightly linked to regional brain metabolism at rest and in response to cognitive tasks (26,27). CBF as measured by ASL has also been shown to provide similar estimates as positron emission tomography without the need for ionizing radiation, making it ideal for use in both pediatric populations and in large scale studies (28,29). The cerebral blood flow quantification parameter uses a venous blood T1 model which accounts for the fact that T1 relaxation time differs according to developmental phase and sex (30). This procedure enhances the accuracy and reliability of results in pediatric samples (31). Alternatively, blood T1 could be measured independently in each participant; however, this approach would be challenging and time-consuming to measure in vivo.

Additionally, empirically measured blood T1 has shown greater test–retest variability compared with relying on a T1 model (31). Our use of a venous blood T1 model for the estimate of arterial blood T1 is based on the similarity of arterial and venous T1 (within 100 ms at 3T). Furthermore, both blood pools show very little dependence over the physiologic range of hemoglobin saturation and both follow a similar dependence on hematocrit level (32); therefore, they are likely to have similar dependence on development- and sex-related changes in blood chemistry.

Group-level Analyses

In order to identify regions where perfusion was related to summary scores of state or trait anxiety, we conducted a whole-brain voxelwise analysis. Both linear and nonlinear age effects were flexibly modeled using penalized splines within a generalized additive model (GAM; 33,34). The GAM assesses a penalty on nonlinearity using restricted maximum likelihood in order to avoid over-fitting, and thus captures both linear and non-linear effects in a data-driven fashion. Because our prior work has demonstrated the presence of nonlinear sex differences in the evolution of cerebral perfusion (8), all models included sex as well as an age-by-sex interaction term. Additionally, because CBF is higher in gray matter than white matter, differences in brain structure could potentially confound analyses of brain perfusion (35). To control for such a confound, gray matter density was calculated from the T1 image segmentation using Atropos (20) and modeled on a voxelwise basis. Finally, as data quality can systematically influence studies of development (22,23), in-scanner motion was also included as a covariate in all analyses as described above. Thus, our complete model was as follows:

$$CBF_{vox} = \text{trait anxiety} + \text{state anxiety} + \text{sex} + \text{spline(age)} + \text{spline(age, by=sex)} + \text{gray matter density}_{vox} + \text{in-scanner motion}$$

where vox = voxels. This model was run at every gray matter voxel within the MNI template where image coverage existed (103,206 2-mm^3 voxels). Type I error for voxelwise whole-brain analyses was controlled using AFNI AlphaSim (36) with a minimum voxel significance of $z > 2.58$ and a corrected cluster significance of $p < .0001$ (minimum cluster size k = 146).

Analyses of Interactions With Age and Puberty

Based on our previous work in this dataset showing that CBF is higher in females than males during puberty (8), we next evaluated whether interactive effects with age and sex were present within regions identified by the voxelwise analysis as anxiety-relevant. Specifically, following the voxelwise analysis, we examined clusters where a significant main effect of anxiety was found, and we modeled interactions between anxiety and age to see if the relationship between perfusion and anxiety increased with age. We also examined the interaction between sex and age in these regions. In regions with a significant trait anxiety-by-age interaction, we examined the relationship between anxiety and pubertal stage (while controlling for age), to determine if the association between perfusion and anxiety strengthened with pubertal stage beyond the effects of age alone. To control for multiple comparisons across clusters, for all analyses we used the false discovery rate ($Q < 0.05$). While three-way interactions were considered, they were not significant and are not discussed further.

Mediation Analysis

As a final step, we investigated whether higher levels of anxiety in females were mediated by higher CBF. Mediation analyses were conducted using the procedures outlined by Preacher and Hayes (37) using IBM SPSS Statistics 22. As described below, sex differences were only found

in trait anxiety in the post-pubertal stage, so mediation analyses focused on this period. Specifically, we examined the total effect of sex on trait anxiety (*c* path; **Figure 4B**), the relationship between sex and perfusion (*a* path), the relationship between perfusion and trait anxiety (*b* path), and the direct effect of sex on trait anxiety after adding perfusion as a mediator to the model (*c*' path). The indirect effect of sex on trait anxiety through the proposed mediator (perfusion) was tested using both the Sobel test and bootstrapping procedures, which make fewer assumptions about the sampling distribution (37). This procedure involves computing unstandardized indirect effects for each of 10,000 bootstrapped samples and calculating the 95% confidence interval.

Sensitivity Analyses

Following the voxelwise analysis described above, we conducted additional analyses in order to assess the influence of other potentially confounding variables. In one analysis, we excluded the minority (12%) of participants who were treated with psychoactive medication at the time of imaging, and additionally included other covariates including race and maternal education (see **Table S6**). Furthermore, in order to exclude the possibility that covariance between state and trait anxiety drove observed results, we conducted additional analyses where they were modeled separately (see **Table S5**). Additionally, we reanalyzed the data using raw scores from STAI data that were not factor analyzed to remove response bias (see **Table S7**).

Connectivity Analyses

As previously detailed (2), resting-state blood oxygen level dependent fMRI was acquired using a whole-brain, single-shot, multi-slice, gradient-echo echoplanar sequence with the following

parameters: 124 volumes, TR 3000 ms, TE 32 ms, flip angle 90°, FOV 192 x 192 mm, matrix 64 x 64, slice thickness/gap 3 mm/0 mm, effective voxel resolution 3.0 x 3.0 x 3.0 mm. During the resting-state scan, a fixation cross was displayed as images were acquired. Participants were instructed to stay awake, keep their eyes open, fixate on the displayed crosshair, and remain still.

Timeseries data were processed using a validated confound regression procedure that has been optimized to reduce the influence of subject motion (38). The first 4 volumes of the functional timeseries were removed to allow signal stabilization, leaving 120 volumes for subsequent analysis, which were re-aligned using MCFLIRT. For use in confound regression, mean white matter (WM) and cerebrospinal fluid (CSF) signals were extracted from tissue segments defined using the T1 image for each subject. Improved confound regression utilized a 36-parameter model, which was composed of 9 standard confounding signals (6 motion parameters + global / WM / CSF) as well as the temporal derivative, quadratic term, and temporal derivative of the quadratic of each. In order to avoid frequency mismatch (39), confound signals and the functional timeseries were band-pass filtered to retain frequencies between 0.01-0.08 Hz. Distortion correction, co-registration to the T1 image, and normalization to the MNI template utilized identical procedures to those used for the ASL scan (see methods in main text).

This pre-processed data was used to conduct seed based connectivity analyses of the left amygdala. The amygdala seed was defined using the cluster where the association between CBF and trait anxiety was found to be present. A Pearson's correlation between the voxel-averaged timeseries of this cluster and every other voxel in the brain was calculated, yielding one correlation map per subject. This correlation map was z-transformed to improve normality, and then evaluated using general additive models that were nearly identical to those used for the ASL

data. However, for resting state data, motion was calculated from the resting-state scan, and gray matter density was not included as a covariate. Cluster correction used the same thresholds as for the ASL data, and interaction analyses (age by sex, trait anxiety by age, and trait anxiety by pubertal stage), and were evaluated within significant clusters.

Table S1. Sample size for each pubertal stage.

Pubertal Stage	***n***
Early-pubertal	139
Mid-pubertal	277
Post-pubertal	452
Missing data	7

Table S2. Factor loadings on the state summary factor of the State-Trait Anxiety Inventory

State Item	Loading[a]
Feel calm	.60
Feel secure	.42
Feel at ease	.50
Feel satisfied	.38
Feel comfortable	.51
Feel self-confident	.38
Relaxed	.63
Feel content	.37
Feel steady	.39
Feel pleasant	.42
Feel tense	.70
Feel strained	.53
Feel upset	.47
Worrying over misfortunes	.58
Feel frightened	.76
Feel nervous	.81
Jittery	.60
Feel indecisive	.47
Worried	.79
Feel confused	.58

[a]All loadings are significant at $p < .05$.

Table S3. Factor loadings on the trait summary factor of the State-Trait Anxiety Inventory

Trait Item	Loading[a]
Feel pleasant	.53
Satisfied with self	.66
Feel rested	.47
Calm, cool, collected	.57
Happy	.65
Feel secure	.56
Make decisions easily	.36
Content	.40
Steady person	.49
Feel nervous and restless	.56
Wish could be happy	.64
Feel like a failure	.65
Difficulties piling up	.58
Worry too much	.59
Have disturbing thoughts	.63
Lack self-confidence	.62
Feel inadequate	.32
Unimportant thoughts	.50
Take disappointments keenly	.39
State of turmoil	.50

[a]All loadings are significant at $p < .05$.

Table S4. Regions where trait anxiety was associated with increased perfusion using a more liberal cluster threshold.

Region	*k*	Maximum *z*	Peak MNI Coordinates		
Fusiform	1036	4.39	-36	-58	-14
Left insula	560	4.00	-44	30	2
Left precentral gyrus	275	3.70	-48	-10	38
Left frontal pole	263	3.82	-26	44	36
Right insula	218	3.99	46	30	-8
Left inferior lateral occipital cortex	193	3.62	-38	-88	-8
Left amygdala	168	3.63	-20	-4	-16
Right frontal pole	148	3.75	30	40	-12
Left lateral occipital cortex	139	3.52	-46	-72	16
Left planum temporale	138	3.7	-56	-22	6
Right precuneus	135	3.39	8	-56	52
Right superior temporal gyrus	115	3.5	52	-8	-14
Dorsal anterior cingulate	112	3.58	-8	26	38

Clusters considered significant if $z > 2.58$, $k > 112$ in a sample of 875 subjects.

Table S5. Voxelwise analyses with state and trait anxiety modeled separately.

Region	*k*	Maximum *z*	Peak MNI Coordinates		
State Anxiety					
Left thalamus	212	3.99	-6	-6	10
Trait Anxiety					
Medial temporal lobe/left amygdala	1447	4.07	-44	-56	-10
Left insula	1217	4.48	-36	30	0
Left frontal pole	625	3.67	-16	46	38
Anterior cingulate gyrus	543	3.59	-8	40	14
Right insula	285	3.72	42	28	2
Left thalamus	210	4.29	-10	-12	12
Left precentral gyrus	200	3.82	-10	-30	50
Precuneus	198	3.39	10	-54	56
Planum temporale	187	3.74	-58	-22	6
Left precentral gyrus	180	3.47	-48	-10	36
Right putamen	152	3.27	32	-6	-8
Right frontal pole	146	3.52	30	36	-14

Clusters considered significant if $z > 2.58$, $k > 146$ in a sample of 875 subjects.

Both analyses included covariates including spline of age, spline of age by sex, in-scanner motion, and voxelwise gray matter density.

Table S6. Sensitivity analyses with race, maternal level of education, and no psychiatric psychotropic medications.

Region	*k*	Maximum *z*	Peak MNI Coordinates		
Fusiform	1320	4.67	-36	-58	-14
Left precentral gyrus	223	3.59	-50	-8	38
Left insula	206	4.08	-44	30	2
Planum temporale	205	3.81	-56	-22	4
Left inferior lateral occipital cortex	183	3.71	-38	-88	-8
Right inferior lateral occipital cortex	162	3.4	54	-68	10
Right superior lateral occipital cortex	161	3.52	26	-66	42

Clusters considered significant if z > 2.58, k > 146 in a sample of 766 subjects.

Table S7. Regions where raw[a] scores on trait anxiety were associated with increased perfusion.

Region	*k*	Maximum *z*	Peak MNI Coordinates		
Fusiform/left amygdala	2943	4.78	-36	-58	-14
Right insula	1359	4.22	46	28	-6
Left insula	709	4.01	-44	30	2
Left planum temporale	269	3.83	-56	-24	4
Right frontal medial cortex	258	3.5	8	38	-14
Right frontal pole	205	4.06	30	40	-12
Right precuneus	193	3.8	10	-54	56

Clusters considered significant if $z > 2.58$, $k > 146$ in a sample of 875 subjects.

[a] Raw scores from STAI data that were not factor analyzed to remove response bias.

Table S8. Differences in CBF between categorical screening groups and typically developing youth within the left amygdala cluster.

Screening Category	*d*
Attention-deficit/hyperactivity disorder	.23
Major depressive disorder	.21
Oppositional defiant disorder	.25
Specific phobias	.21
Psychosis	.16
Posttraumatic stress disorder	.30
Social anxiety	.15

d = covariate-adjusted Cohen's *d.*

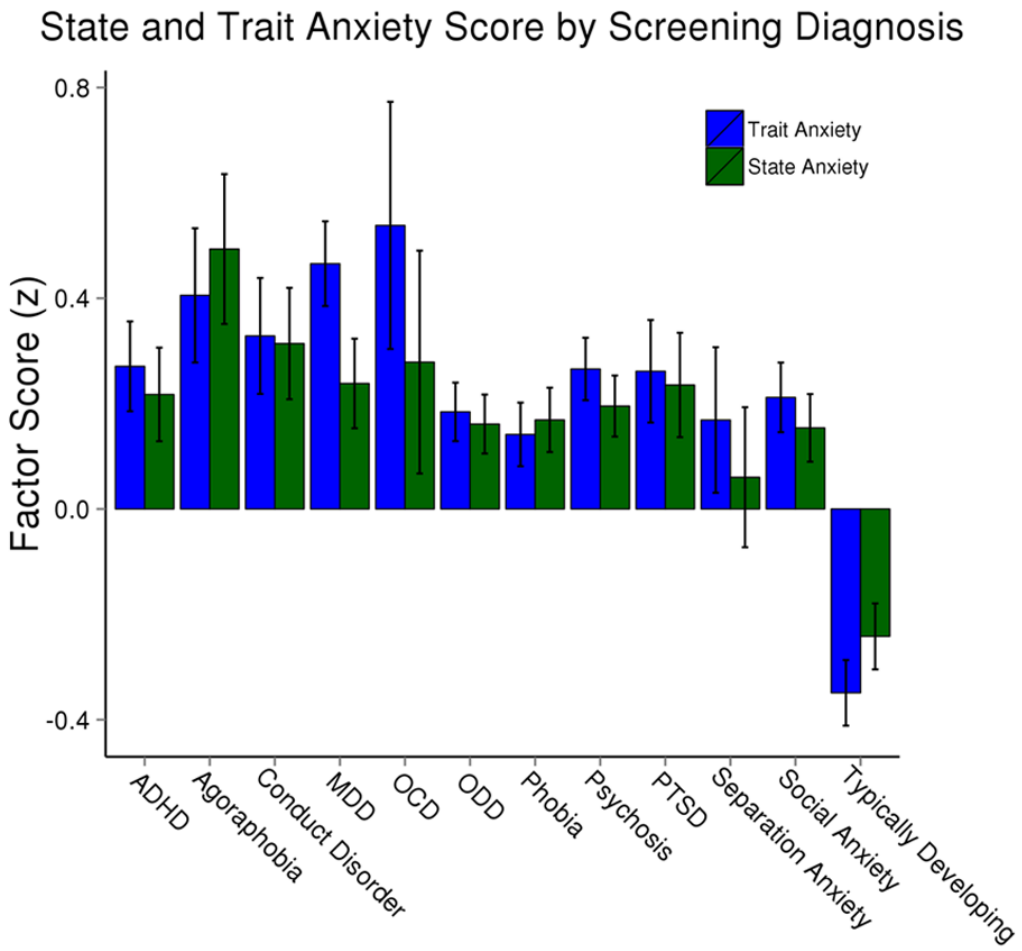

Figure S1. State and trait anxiety by screening diagnostic category. Higher levels of state and trait anxiety were found across all categories compared to typically developing youth. State and trait anxiety represent the summary factors derived from the factor analyses of the items from each scale. Mean (SEM) factor scores for each screening category are presented for categories with at least 20 subjects. ADHD, attention-deficit/hyperactivity disorder; MDD, major depressive disorder; OCD, obsessive-compulsive disorder; ODD, oppositional defiant disorder; PTSD, posttraumatic stress disorder.

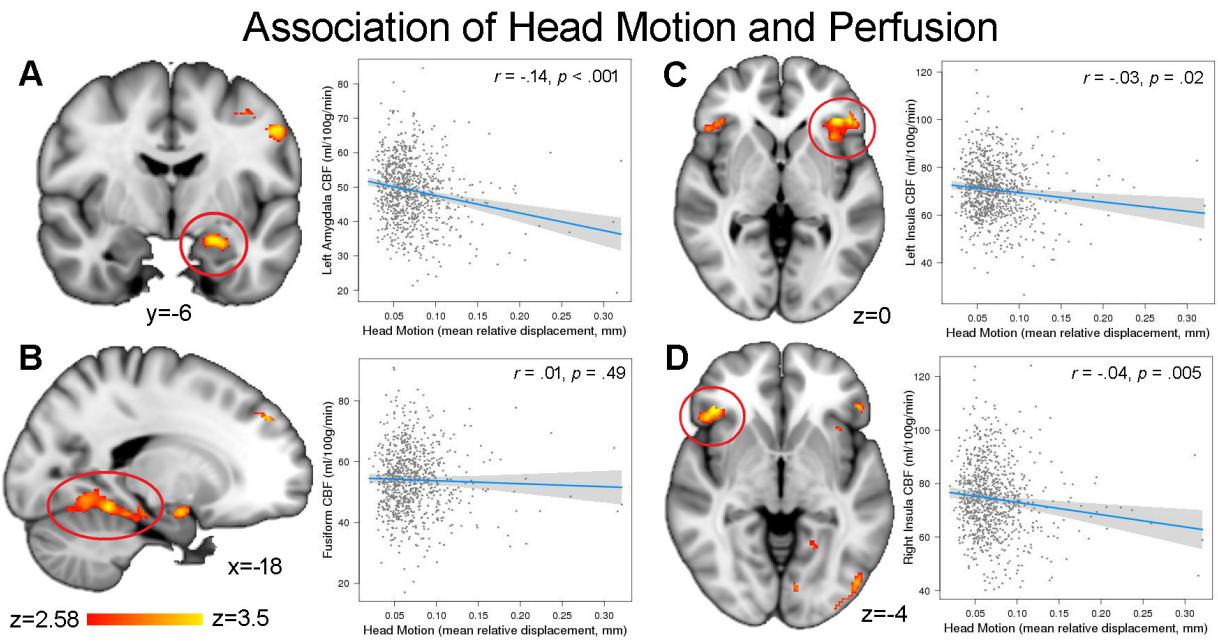

Figure S2. Lower perfusion associated with head motion. Greater head motion was associated with lower perfusion in the (**A**) left amygdala, (**C**) left anterior insula, and (**D**) right anterior insula but not in the (**B**) fusiform gyrus.

Supplementary References

1. Calkins ME, Merikangas KR, Moore TM, Burstein M, Behr MA, Satterthwaite TD, *et al.* (2015): The Philadelphia Neurodevelopmental Cohort: constructing a deep phenotyping collaborative. *Journal of Child Psychology and Psychiatry* 56:1356-1369.
2. Satterthwaite TD, Elliott MA, Ruparel K, Loughead J, Prabhakaran K, Calkins ME, *et al.* (2014): Neuroimaging of the Philadelphia neurodevelopmental cohort. *Neuroimage* 86:544-553.
3. Calkins ME, Moore TM, Merikangas KR, Burstein M, Satterthwaite TD, Bilker WB, *et al.* (2014): The psychosis spectrum in a young US community sample: findings from the Philadelphia Neurodevelopmental Cohort. *World Psychiatry* 13:296-305.
4. Satterthwaite TD, Connolly JJ, Ruparel K, Calkins ME, Jackson C, Elliott MA, *et al.* (2016): The philadelphia neurodevelopmental cohort: a publicly available resource for the study of normal and abnormal brain development in youth. *Neuroimage* 124:1115-1119.
5. Kaufman J, Birmaher B, Brent D, Rao UMA, Flynn C, Moreci P, *et al.* (1997): Schedule for affective disorders and schizophrenia for school-age children-present and lifetime version (K-SADS-PL): initial reliability and validity data. *Journal of the American Academy of Child & Adolescent Psychiatry* 36:980-988.
6. American Psychiatric Association (2000): *Diagnostic and Statistical Manual of Mental Disorders: DSM-IV-TR.* American Psychiatric Association.
7. Morris NM, Udry JR (1980): Validation of a self-administered instrument to assess stage of adolescent development. *Journal of youth and adolescence* 9:271-280.
8. Satterthwaite TD, Shinohara RT, Wolf DH, Hopson RD, Elliott MA, Vandekar SN, *et al.* (2014): Impact of puberty on the evolution of cerebral perfusion during adolescence. *Proceedings of the National Academy of Sciences* 111:8643-8648.
9. Bados A, Gómez-Benito J, Balaguer G (2010): The state-trait anxiety inventory, trait version: does it really measure anxiety? *Journal of personality assessment* 92:560-567.
10. Balsamo M, Romanelli R, Innamorati M, Ciccarese G, Carlucci L, Saggino A (2013): The state-trait anxiety inventory: shadows and lights on its construct validity. *Journal of Psychopathology and Behavioral Assessment* 35:475-486.
11. Reise SP, Moore TM, Haviland MG (2010): Bifactor models and rotations: Exploring the extent to which multidimensional data yield univocal scale scores. *Journal of personality assessment* 92:544-559.
12. Holzinger KJ, Swineford F (1937): The bi-factor method. *Psychometrika* 2:41-54.
13. Muthén LK, Muthén BO (2012): Mplus. *The comprehensive modelling program for applied researchers: Users guide* 5.
14. Reise SP (2012): The rediscovery of bifactor measurement models. *Multivariate Behavioral Research* 47:667-696.
15. Wu W-C, Fernández-Seara M, Detre JA, Wehrli FW, Wang J (2007): A theoretical and experimental investigation of the tagging efficiency of pseudocontinuous arterial spin labeling. *Magnetic Resonance in Medicine* 58:1020-1027.
16. Jenkinson M, Beckmann CF, Behrens TE, Woolrich MW, Smith SM (2012): Fsl. *Neuroimage* 62:782-790.

17. Smith SM (2002): Fast robust automated brain extraction. *Human brain mapping* 17:143-155.
18. Jenkinson M, Bannister P, Brady M, Smith S (2002): Improved optimization for the robust and accurate linear registration and motion correction of brain images. *Neuroimage* 17:825-841.
19. Greve DN, Fischl B (2009): Accurate and robust brain image alignment using boundary-based registration. *Neuroimage* 48:63-72.
20. Avants BB, Tustison NJ, Song G, Cook PA, Klein A, Gee JC (2011): A reproducible evaluation of ANTs similarity metric performance in brain image registration. *Neuroimage* 54:2033-2044.
21. Klein A, Andersson J, Ardekani BA, Ashburner J, Avants B, Chiang M-C, *et al.* (2009): Evaluation of 14 nonlinear deformation algorithms applied to human brain MRI registration. *Neuroimage* 46:786-802.
22. Satterthwaite TD, Wolf DH, Loughead J, Ruparel K, Elliott MA, Hakonarson H, *et al.* (2012): Impact of in-scanner head motion on multiple measures of functional connectivity: relevance for studies of neurodevelopment in youth. *Neuroimage* 60:623-632.
23. Satterthwaite TD, Wolf DH, Ruparel K, Erus G, Elliott MA, Eickhoff SB, *et al.* (2013): Heterogeneous impact of motion on fundamental patterns of developmental changes in functional connectivity during youth. *Neuroimage* 83:45-57.
24. Aguirre GK, Detre JA (2012): The development and future of perfusion fMRI for dynamic imaging of human brain activity. *NeuroImage* 62:1279-1285.
25. Detre, John A (2012): Physiology of Functional Activation. In: Wilson DF, Evans SM, Biaglow J, Pastuszko A, editors. *Oxygen Transport To Tissue XXIII: Oxygen Measurements in the 21st Century: Basic Techniques and Clinical RelevanceVolume 510 of Advances in Experimental Medicine and Biology*. Springer Science & Business Media, pp 365-368.
26. He X, Raichle ME, Yablonskiy DA (2012): Transmembrane dynamics of water exchange in human brain. *Magnetic resonance in medicine* 67:562-571.
27. Detre JA, Rao H, Wang DJ, Chen YF, Wang Z (2012): Applications of arterial spin labeled MRI in the brain. *Journal of Magnetic Resonance Imaging* 35:1026-1037.
28. Xu G, Rowley HA, Wu G, Alsop DC, Shankaranarayanan A, Dowling M, *et al.* (2010): Reliability and precision of pseudo-continuous arterial spin labeling perfusion MRI on 3.0 T and comparison with 15O-water PET in elderly subjects at risk for Alzheimer's disease. *NMR in Biomedicine* 23:286-293.
29. Ye FQ, Berman KF, Ellmore T, Esposito G, van Horn JD, Yang Y, *et al.* (2000): H215O PET validation of steady-state arterial spin tagging cerebral blood flow measurements in humans. *Magnetic Resonance in Medicine* 44:450-456.
30. Wu W-C, Jain V, Li C, Giannetta M, Hurt H, Wehrli FW, *et al.* (2010): In vivo venous blood T1 measurement using inversion recovery true-FISP in children and adults. *Magnetic Resonance in Medicine* 64:1140-1147.
31. Jain V, Duda J, Avants B, Giannetta M, Xie SX, Roberts T, *et al.* (2012): Longitudinal reproducibility and accuracy of pseudo-continuous arterial spin--labeled perfusion MR imaging in typically developing children. *Radiology* 263:527-536.

32. Lu H, Clingman C, Golay X, van Zijl P (2004): Determining the longitudinal relaxation time (T1) of blood at 3.0 Tesla. *Magnetic resonance in medicine* 52:679-682.

33. Wood SN (2004): Stable and efficient multiple smoothing parameter estimation for generalized additive models. *Journal of the American Statistical Association* 99:673-686.

34. Wood SN (2011): Fast stable restricted maximum likelihood and marginal likelihood estimation of semiparametric generalized linear models. *Journal of the Royal Statistical Society: Series B (Statistical Methodology)* 73:3-36.

35. Taki Y, Hashizume H, Sassa Y, Takeuchi H, Wu K, Asano M, *et al.* (2011): Correlation between gray matter density-adjusted brain perfusion and age using brain MR images of 202 healthy children. *Human brain mapping* 32:1973-1985.

36. Cox RW (1996): AFNI: software for analysis and visualization of functional magnetic resonance neuroimages. *Computers and Biomedical research* 29:162-173.

37. Preacher KJ, Hayes AF (2008): Asymptotic and resampling strategies for assessing and comparing indirect effects in multiple mediator models. *Behavior research methods* 40:879-891.

38. Satterthwaite TD, Elliott MA, Gerraty RT, Ruparel K, Loughead J, Calkins ME, *et al.* (2013): An improved framework for confound regression and filtering for control of motion artifact in the preprocessing of resting-state functional connectivity data. *Neuroimage* 64:240-256.

39. Hallquist MN, Hwang K, Luna B (2013): The nuisance of nuisance regression: spectral misspecification in a common approach to resting-state fMRI preprocessing reintroduces noise and obscures functional connectivity. *Neuroimage* 82:208-225.